**Naval Research Laboratory**
Washington, DC 20375-5320

**NRL/6041/MR—2022/2**

# Development of a Model Verification Test Case for Chemically Reacting Flows: Mixing Layer Interacting with an Impinging Oblique Shock

SARAH K. BURROWS

*Rensselaer Polytechnic Institute*
*Troy, New York*

RYAN F. JOHNSON

ERIC J. CHING

*Laboratory for Propulsion, Energetic, and Dynamic Systems*
*Laboratories for Computational Physics and Fluid Dynamics*

October 4, 2022

# REPORT DOCUMENTATION PAGE

*Form Approved*
*OMB No. 0704-0188*



| **1. REPORT DATE** *(DD-MM-YYYY)* | **2. REPORT TYPE** | **3. DATES COVERED** *(From - To)* |
|---|---|---|
| 04-10-2022 | NRL Memorandum Report | May 31, 2022 – September 22, 2022 |

**4. TITLE AND SUBTITLE**

Development of a Model Verification Test Case for Chemically Reacting Flows: Mixing Layer Interacting with an Impinging Oblique Shock

**5a. CONTRACT NUMBER**

**5b. GRANT NUMBER**

**5c. PROGRAM ELEMENT NUMBER**

**6. AUTHOR(S)**

Sarah K. Burrows*, Ryan F. Johnson, Eric. J. Ching

**5d. PROJECT NUMBER**

**5e. TASK NUMBER**

**5f. WORK UNIT NUMBER**
1Y52

**7. PERFORMING ORGANIZATION NAME(S) AND ADDRESS(ES)**

Naval Research Laboratory
4555 Overlook Avenue, SW
Washington, DC 20375-5320

**8. PERFORMING ORGANIZATION REPORT NUMBER**

NRL/6041/MR--2022/2

**9. SPONSORING / MONITORING AGENCY NAME(S) AND ADDRESS(ES)**

Naval Research Laboratory
4555 Overlook Avenue, SW
Washington, DC 20375-5320

**10. SPONSOR / MONITOR'S ACRONYM(S)**

NRL

**11. SPONSOR / MONITOR'S REPORT NUMBER(S)**

**12. DISTRIBUTION / AVAILABILITY STATEMENT**

**DISTRIBUTION STATEMENT A:** Approved for public release; distribution is unlimited.

**13. SUPPLEMENTARY NOTES**

*Rensselaer Polytechnic Institute, 110 8th St, Troy, NY 12180

**14. ABSTRACT**

In this memorandum, we document the development of a verification test case for the chemically reacting, multi-component Navier-Stokes equations. We seek a configuration that contains the physics of interest to simulating high-speed propulsion devices. These devices contain diverse phenomena, including unsteady multidimensional fluid dynamics, convective and thermal diffusive layers, wrinkled flames, oblique shocks, and expansion waves. The objective test case should be used to demonstrate the capabilities of developed numerical methods and showcase those methods do not compromise the fidelity of the physics due to invasive stabilization techniques. The development of numerical test cases is not always straight forward, so we document our experience historically and present the final configuration: a chemically reacting shear layer in the presence of an oblique shock. We present the mesh, boundary conditions, and final, reproducible result for both two-dimensional and three dimensional configurations. This will help the combustion community in supplying a test case that any multicomponent chemically reacting compressible Navier Stokes solver should be able to reproduce. Additionally, the accurate simulation and demonstration of these physics with a reproducible test case is important for future work in the field of high speed-propulsion. Simulations were performed using the JENRE® Multiphysics Framework with extensions for numerical stability still currently in development at the Naval Research Laboratory.

**15. SUBJECT TERMS**

| **16. SECURITY CLASSIFICATION OF:** | | | **17. LIMITATION OF ABSTRACT** | **18. NUMBER OF PAGES** | **19a. NAME OF RESPONSIBLE PERSON** |
|---|---|---|---|---|---|
| | | | | | Ryan F. Johnson |
| **a. REPORT** | **b. ABSTRACT** | **c. THIS PAGE** | U | 23 | **19b. TELEPHONE NUMBER** *(include area code)* |
| U | U | U | | | (520) 272-4397 |

**Standard Form 298 (Rev. 8-98)**
**Prescribed by ANSI Std. Z39.18**

This page intentionally left blank.

## CONTENTS

## FIGURES

## TABLES

This page intentionally left blank

# EXECUTIVE SUMMARY

A verification test case for the chemically reacting, multi-component Navier-Stokes equations is developed. The test case can be used to demonstrate the capabilities of developed numerical methods and showcase those methods do not compromise the fidelity of the physics due to invasive stabilization techniques

This page intentionally left blank

# DEVELOPMENT OF A MODEL VERIFICATION TEST CASE FOR CHEMICALLY REACTING FLOWS: MIXING LAYER INTERACTING WITH AN IMPINGING OBLIQUE SHOCK

## 1. REVIEW OF METHODS AND EXISTING TEST CASES

Modeling multicomponent, chemically reacting, compressible flows have inherent difficulties. The mixing of species with different thermodynamic properties, wether it be numerical or physical, can cause unphysical pressure oscillations that often lead to failure of the simulation as reviewed in [1, 2] in the context high order finite element methods. In [3], we presented a discontinuous Galerkin method that remains conservative and preserves pressure equilibrium with documentation over a variety of test cases. We also showed that simulating the sharp continuous gradients in the flame regions has inherent difficulties, requiring fine mesh sizes or higher-order elements to resolve the flame structures.

Beyond sharp gradients is the need to capture shocks and detonations. The legacy approach is to utilize numerical schemes that smear the discontinuities to represent them continuously, however it is hard to guarantee to not destroy solution accuracy in regions away from these features. In [3] we introduced an artificial viscosity which used a shock sensor developed by [4]. That numerical scheme was used effectively to suppress spurious oscillations in the vicinity of flow-field discontinuities in multicomponent reacting flows.

In addition to the transport phenomena, stiff chemical kinetics interact with the flow, resulting in the need to resolve a complex reactions that contribute to the nonlinear source terms. In [3], we presented an $hp$-adaptive DG method for solving systems of ordinary differential equations, DGODE, which is used to resolve the temporal evolution of the species concentrations due to stiff chemical reactions.

There are a variety of test cases that have been developed for demonstrating the ability to simulate chemically reacting, compressible flows and maintain stability. In [2, 3, 5] the approximate interaction of shocks with multi-component non-reacting gases between helium and air were presented. This test case was used to demonstrate shock capturing techniques without the presence of chemical reaction or physical diffusion, but included the different thermodynamic properties of the species modeled. Expanding on these test cases, [2, 3, 5] also presented sustained detonations formed in hydrogen-air mixtures. These cases coupled compressible phenomena, shocks and detonations, with chemical reactions but did not include the effects of physical diffusion.

Various demonstration cases have been used to couple convective and diffusive transport with the detailed chemical source terms. In [2, 3, 5, 6] a one-dimensional freely propagating flame was simulated that included the presence of chemical reaction, diffusion, and convective terms, however no shocks or detonations were present in those cases. Additionally, in [3] a subsonic, chemically reacting shear layer case was approximated in two and three-dimensions.

Manuscript approved September 29, 2022.

In this memorandum, we document the development of a verification case that can demonstrate a numerical method's ability to approximate the physics of interest in multicomponent, chemically reacting, compressible flows. The field of high-order numerics is consistently producing new methods to model these types of flows and an additional test case is a valuable contribution.

We require that the test case must be multidimensional to demonstrate the numerical method is general. Due to the compressible formulation, the test case must involve shocks to demonstrate the numerical method can stabilize discontinuities. In order to demonstrate the numerical method can resolve physical diffusive fluxes, such as species diffusion and viscous, the test case must involve shear-layers and species-mixing. The test case must utilize detailed chemistry, thermodynamics, and transport in order to assure the method can approximate the physics to the highest physical fidelity as possible; no compromises can be made in the physics to achieve stability. Finally, the test case must involve unstructured grids, thus demonstrating the numerical method does not require specialized grids in order to achieve a stable solution.

Here we build off an existing test case presented in [6] that intersects a chemically reacting shear layer with an oblique shock. We expand the geometry to include a ramp that creates the oblique shock. This is different than the original case, which specified the a fluid dynamic state at the boundaries to create an oblique shock. We also introduce a length scale parameter to test both steady and unsteady configurations. We approximate the flow on an unstructured grid in two and three dimensions. We use a combination of sine functions to introduce unsteadiness in time instead of using a white noise generator like in [6]. This assures reproducibility with the unsteadiness that would not be obtainable with a random perturbations in the configuration. Simulations were performed using the JENRE® Multiphysics Framework building of the formulation of Johnson and Kercher [3] with additional extensions for numerical stability still currently in development at the Naval Research Laboratory.

## 2. THE MULTICOMPONENT CHEMICALLY REACTING NAVIER STOKES EQUATIONS

Here we repeat the multicomponent chemically reacting Navier Stokes equations as presented in [3]. Let $\Omega \subset \mathbb{R}^d$ be a given $d$-dimensional domain with boundary $\partial\Omega$, over which an outward oriented normal $n : \partial\Omega \to \mathbb{R}^d$ is defined, and $T \subset \mathbb{R}^+$ is a given temporal interval. The nonlinear conservation law governing the unsteady chemically reacting Navier-Stokes equations, in strong form, defined for piecewise smooth, $\mathbb{R}^m$-valued functions $y$, and gradient $\nabla y$, is given as

$$\frac{\partial y}{\partial t} + \nabla \cdot \mathcal{F}\left(y, \nabla y\right) - \mathcal{S}\left(y\right) = 0 \text{ in } \Omega \times T, \tag{1}$$

$$y\left(\cdot, t_0\right) - y_0 = 0 \text{ in } \Omega, \tag{2}$$

$$n \cdot \mathcal{F}\left(y, \nabla y\right) - n \cdot \mathcal{F}_{\partial}\left(y, \nabla y\right) = 0 \text{ on } \partial\Omega \times T, \tag{3}$$

$$G_{\partial}\left(y_{\partial}\right) : \left(y^{+} - y_{\partial}\right) \otimes n = 0 \text{ on } \partial\Omega \times T, \tag{4}$$

where $t$ denotes time, $\mathcal{F} : \mathbb{R}^m \to \mathbb{R}^{m \times d}$ is a given flux function, $\mathcal{S} : \mathbb{R}^m \to \mathbb{R}^m$ is a given source term. The initial conditions at time $t_0$ are given by $y_0$ in Equation (2). The flux function

$$F\left(y, \nabla y\right) = \left(\mathcal{F}^c\left(y\right) - \mathcal{F}^v\left(y, \nabla y\right)\right) \tag{5}$$

is defined in terms of the convective flux $\mathcal{F}^c(y)$, which is only a function of the state $y$, and viscous flux $\mathcal{F}^v(y, \nabla y)$, which is a function of the state and the gradient, $\nabla y$. Furthermore, the viscous flux can be written as

$$\mathcal{F}^v(y, \nabla y) = G(y) : \nabla y \tag{6}$$

where $G(y) = \mathcal{F}^v_{\nabla y}$ is its the partial linearization with respect to the gradient, $\nabla y$, which is sometimes referred to as the homogeneity tensor [7].

The chemically reacting Navier-Stokes flow state variable is given by

$$y = \left(\rho v_1, \ldots, \rho v_d, \rho e_t, C_i, \ldots, C_{n_s}\right), \tag{7}$$

where $m = d + n_s + 1$, $n_s$ is the number of thermally perfect species, $\rho : \mathbb{R}^{n_s} \to \mathbb{R}$ is density, $(v_1, \ldots, v_d) : \mathbb{R}^m \to \mathbb{R}^d$ is the velocity, $e_t : \mathbb{R}^m \to \mathbb{R}$ is the specific total energy, and $C : \Omega \to \mathbb{R}^{n_s}$ are the species concentrations. The density is calculated from the concentrations as

$$\rho = \sum_{i=1}^{n_s} W_i C_i, \tag{8}$$

where $W_i$ is the molecular weight of species $i$.

The $k$-th spatial convective flux component is given by

$$\mathcal{F}^c_k(y) = \left(\rho v_k v_1 + p\delta_{k1}, \ldots, \rho v_k v_d + p\delta_{kd}, v_k(\rho e_t + p), v_k C_1, \ldots, v_k C_{n_s}\right). \tag{9}$$

The pressure, $p : \mathbb{R}^m \to \mathbb{R}$, is calculated from the equation of state,

$$p = R^0 T \sum_{i=1}^{n_s} C_i, \tag{10}$$

where $T : \mathbb{R}^m \to \mathbb{R}$, is the temperature and $R^0 = 8314.4621\,\mathrm{JKmol^{-1}K^{-1}}$ is the universal gas constant. The total energy, $\rho e_t$, is given as the sum of the internal and kinetic and energies as

$$\rho e_t = \rho u + \frac{1}{2} \sum_{k=1}^{d} \rho v_k v_k, \tag{11}$$

where $\rho u : \mathbb{R}^m \to \mathbb{R}$ is the internal energy. The internal energy is also defined as the mass weighted sum of thermally perfect species specific internal energies that are $n_p$-order polynomials with respect to temperature,

$$\rho u = \sum_{i=1}^{n_s} W_i C_i \sum_{k=0}^{n_P} a_{ik} T^k. \tag{12}$$

In this work, all thermodynamic polynomials are continuous refits of the analytic form from NASA's polynomial representations [8].

The $k$-th spatial component of the viscous flux is given by

$$\mathcal{F}_k^v\left(y, \nabla y\right) = \left(\tau_{1k}, \ldots, \tau_{dk}, \sum_{j=1}^{d} \tau_{kj} v_j - W_i C_i h_i V_{ik} - q_k, C_1 V_{1k}, \ldots, C_{n_s} V_{n_s k}\right), \tag{13}$$

where $q : \mathbb{R}^m \times \mathbb{R}^{m\times d} \to \mathbb{R}^d$ is the thermal heat flux, $\tau : \mathbb{R}^m \times \mathbb{R}^{m\times d} \to \mathbb{R}^{d\times d}$ is the viscous stress tensor, $\left(h_1, \ldots, h_{n_s}\right) : \mathbb{R}^m \to \mathbb{R}^{n_s}$ are the species specific enthalpies, and $\left(\left(V_{11}, \ldots, V_{1d}\right), \ldots, \left(V_{n_s 1}, \ldots, V_{n_s d}\right)\right) : \mathbb{R}^m \times \mathbb{R}^{n_s\times d} \to \mathbb{R}^{n_s\times d}$ are the species diffusion velocities. The $k$-th spatial component of the viscous stress tensor is given by

$$\tau_k\left(y, \nabla y\right) = \mu\left(\frac{\partial v_1}{\partial x_k} + \frac{\partial v_k}{\partial x_1} - \delta_{k1}\frac{2}{3}\sum_{j=1}^{d}\frac{\partial v_j}{\partial x_j}, \ldots, \frac{\partial v_d}{\partial x_k} + \frac{\partial v_k}{\partial x_d} - \delta_{kd}\frac{2}{3}\sum_{j=1}^{d}\frac{\partial v_j}{\partial x_j}\right), \tag{14}$$

where $\mu : \mathbb{R}^m \to \mathbb{R}$ is the dynamic viscosity. The $k$-th spatial component of the heat flux is given as

$$q_k\left(y, \nabla y\right) \quad = \quad -\lambda\frac{\partial T}{\partial x_k}.$$

where $\lambda : \mathbb{R}^m \to \mathbb{R}$ is the thermal conductivity.

The transport properties are calculated using mixture averaged properties. The $k$-th spatial component of the diffusion velocity for the $i$-th species is given as

$$V_{ik}^{\dagger} = \frac{\bar{D}_i}{C_i}\frac{\partial C_i}{\partial x_k} - \frac{\bar{D}_i}{\rho}\frac{\partial \rho}{\partial x_k}. \tag{15}$$

To ensure mass conservation, i.e. $\sum_{i=1}^{n_s} W_i C_i V_{ik} = 0$, a standard correction, see [9] and [5], is applied to the species diffusion velocity (15),

$$V_{ik} = V_{ik}^{\dagger} - \frac{\sum_{i=1}^{n_s} W_i C_i V_{ik}^{\dagger}}{\rho}. \tag{16}$$

The species mixture averaged diffusion coefficients $\left(\bar{D}_1, \ldots, \bar{D}_{n_s}\right) : \mathbb{R}^m \rightarrow \mathbb{R}^{n_s}$, from [10], are defined for the $i$-th species as

$$\bar{D}_i = \frac{p_{atm}}{p\bar{W}} \frac{\sum_{j=1, j\neq i}^{n_s} X_j W_j}{\sum_{j=1, j\neq i}^{n_s} X_j / D_{ij}}, \tag{17}$$

where $p_{atm} = 101325$ Pa, $X_j$ is the mole fraction of species $j$, $D_{ij}$ is the diffusion coefficient of species $i$ to species $j$, and $\bar{W} : \mathbb{R}^m \rightarrow \mathbb{R}$ is the mixture molecular weight, defined as

$$\bar{W} = \frac{\rho}{\sum_{i=1}^{n_s} C_i}. \tag{18}$$

and the mole fractions $\left(X_1, \ldots, X_{n_s}\right) : \mathbb{R}^{n_s} \rightarrow \mathbb{R}^{n_s}$ can be calculated directly from concentrations,

$$X_i = \frac{C_i}{\sum_{i=1}^{n_s} C_i}. \tag{19}$$

The Wilke model [11] is used to calculate viscosity

$$\mu = \sum_{i=1}^{n_s} \frac{X_i \mu_i}{X_i + \sum_{i=1, i\neq j}^{n_s} \left(X_j \phi_{ij}\right)}, \tag{20}$$

where

$$\phi_{ij} = \frac{\left(1 + \left(\frac{W_j}{W_i}\right)^{1/4} \sqrt{\left(\frac{\mu_i}{\mu_j}\right)}\right)^2}{\sqrt{8\left(1 + \frac{W_i}{W_j}\right)}},$$

and $\mu_i$ and $\mu_j$ are the species specific viscosities for species $i$ and $j$, respectively. The Mathur model [12] is used to calculate conductivity,

$$\lambda = \frac{1}{2}\left(\sum_{i=1}^{n_s} X_i \lambda_i + \frac{1}{\sum_{i=1}^{n_s} \frac{X_i}{\lambda_i}}\right), \tag{21}$$

where $\lambda_i$ is the conductivity of species $i$.

Finally, the source term, which includes the detailed chemical kinetics, is given by

$$\mathcal{S}(y) = \left(0, \ldots, 0, 0, \omega_1, \ldots, \omega_{n_s}\right), \tag{22}$$

where $\omega_i$ is the production rate of species $i$, which is the sum of the progress reaction rates from any arbitrary number of reactions and reaction types, cf. [13].

## 3. TEST CASE DESCRIPTION AND BOUNDARY CONDITIONS

Figures 1 displays a diagram of the two dimensional configuration. Fuel and air enter the domain on the left hand side at supersonic speeds creating a mixing layer, shown in green. At the prescribed conditions, listed in Table 1, reactions automatically occur creating a chemical reaction zone that persists downstream. The supersonic air meets a ramp at angle $\alpha = 5.79^o$ that, at these conditions, has known oblique shock angle $\beta = 33.0^o$, which was chosen to match [6]. The oblique shock intersects with the reacting layer and bends due to a change in gas properties. The oblique shock reflects off the upper wall, bends again in the mixing layer, then exits the domain.

The fuel and air boundary conditions are listed in Table 1 which are prescribed supersonic inflow and do not require any information from the interior domain. The slip wall conditions require that the flow be parallel to the boundary as described in [3]. At the outflow condition no restrictions are applied as the flow is supersonic. For this test case we do not think it is necessary to resolve the boundary layer along the bottom or top walls, as we only wish to generate an oblique shock. Although we still apply the physical diffusion operator to resolve the chemically reacting mixing layer.

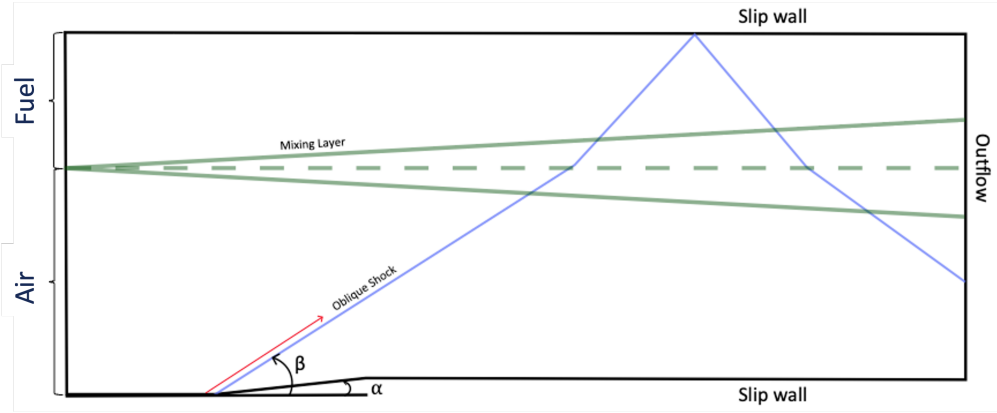


Fig. 1—Domain and boundary condition labels for the objective test case. Inflow is supersonic on the left and outflow is supersonic on the right. Walls are prescribed slip walls as we do not wish to resolve momentum boundary layers.

The inflow boundary conditions are taken from [6]. The high water content and presence of radicals were most likely included to simulate a vitiated air stream. Additionally we found that combustion did not initiate in the mixing layer without the presence of these radicals. We used the detailed reaction mechanism from Westbrook 1982 [14] to calculate the developed solution presented here. We did try the detailed mechanism from [15] as presented in [6], however, there was no qualitative difference for the type of test case we are pursuing and the Westbrook 1982 model was slightly smaller in computational efficiency due to less reactions.

| **Prescribed Quantity** | **Air Boundary** | **Fuel Boundary** |
|---|---|---|
| Veloxity, $v_1$ [m/s] | 1634 m/s | 973 m/s |
| Temperature, $T$ [K] | 1475 | 545 |
| $Y_{O_2}$ | 0.278 | 0 |
| $Y_{N_2}$ | 0.552 | 0.95 |
| $Y_{H_2}$ | 0 | 0.05 |
| $Y_{H_2O}$ | 0.17 | 0 |
| $Y_H$ | $5.6 \times 10^{-7}$ | 0 |
| $Y_O$ | $1.55 \times 10^{-4}$ | 0 |
| $Y_{OH}$ | $1.83 \times 10^{-3}$ | 0 |
| $Y_{HO_2}$ | $5.1 \times 10^{-6}$ | 0 |
| $Y_{H_2O_2}$ | $2.5 \times 10^{-6}$ | 0 |

Table 1—Air and Fuel boundary conditions. Boundary conditions are taken from [6]. The air boundary has radicals included as well as high water content, most likely to simulate a vitiated air stream. Without the radicals combustion did not initiate in the mixing region.

To connect the fuel and air streams we utilize a hyperbolic tangent function to connect the species, temperature, and normal direction velocity with a constant pressure specification,

$$\begin{aligned}
Y_i(x_1,\ldots,x_d,t) &= \frac{1}{2}\left(\left(Y_{i,F}+Y_{i,O}\right)+\left(Y_{i,F}-Y_{i,O}\right)\tanh\left(\frac{\left(2\left(x_2-h\left(x_1,\ldots,x_d,t\right)\right)\right)}{L\left(x_1,\ldots,x_d,t\right)}\right)\right)\\
T(x_1,\ldots,x_d,t) &= \frac{1}{2}\left(\left(T_F+Y_O\right)+\left(T_F-T_O\right)\tanh\left(\frac{\left(2\left(x_2-h\left(x_1,\ldots,x_d,t\right)\right)\right)}{L\left(x_1,\ldots,x_d,t\right)}\right)\right)\\
v_1(x_1,\ldots,x_d,t) &= \frac{1}{2}\left(\left(v_{1,F}+v_{1,O}\right)+\left(v_{1,F}-v_{1,O}\right)\tanh\left(\frac{\left(2\left(x_2-h\left(x_1,\ldots,x_d,t\right)\right)\right)}{L\left(x_1,\ldots,x_d,t\right)}\right)\right)\\
p &= 94232.25 \text{ Pa.}
\end{aligned} \tag{23}$$

Where subscript $O$ is for the air boundary and $F$ is for the fuel side. We did initially try to connect the two conserved states instead of connecting primitive variables, but the connecting of states did not guarantee pressure equilibrium. Inflow, weak, oblique shocks were noticed by not assuring pressure equilibrium which is apparent in initial solutions shown in the length scale investigation in Subsection 4.1.

In Equation 23 we created functions for length scale, $L$, and hyperbolic tangent center, $h$. This made it easier to induce unsteady features and variation in the three dimensional case. For the length scale we specify a Fourier sine series

$$\begin{aligned}
L(x_1,\ldots,x_d,t) &= L_s+\sum_{i=1}^{n_t}A_i\sin\left(\frac{n_i 2\pi t}{t_r}\right)+l(x_1,\ldots,x_d)\\
l\left(x_1,\ldots,x_d\right) &= \sum_{i=1}^{n_v}B_i\sin\left(\frac{m_i 2\pi x_3}{z_h}\right)\sum_{i=1}^{n_w}C_i\sin\left(\frac{q_i 2\pi t}{t_r}\right) \text{ if } d>2,
\end{aligned} \tag{24}$$

where $L_s$ is the ambient length scale; $A_i$,$B_i$, and $C_i$ are amplitudes; and $n_i$, $m_i$, and $q_i$ are wave numbers; $z_h$ is the simulation domain thickness in the $z$-direction; and $t_r$ is a specified time scale, in this case the flow-through time according to the air velocity. In [6] a white noise generator was used in the bottom domain boundary to produce unsteadiness. We chose a series of sine functions in order to invoke unsteadiness but maintain reproducibility. To encourage variation in the three-dimensional cases we also include a function for the center of the hyperbolic tangent function,

$$h(x_1, \ldots, x_d, t) = h_s + h_t \sin\left(\frac{6\pi t}{z_h t_r}\right)\left(\sin\left(\frac{2\pi x_3}{z_h}\right) + \sin\left(\frac{8\pi x_3}{z_h}\right)\right) \text{ if } d > 2, \tag{25}$$

where $h_s$ is the ambient center of the hyperbolic tangent and $z_h$ is the thickness of the extended domain in the $x_3$-direction.

Figure 2 shows the specifications that were used in gmsh [16] to create an unstructured, triangular mesh. The first two numbers are the $x_1$ and $x_2$ locations of the points of the mesh. A letter is used to indicate the mesh size. After several iterations on mesh size we concluded that the parameters $a = 500 \times 10^{-6}$ m, $b = 200 \times 10^{-6}$ , $c = 60 \times 10^{-6}$ , and $d = 120 \times 10^{-6}$ were sufficient for DG ($p = 2$) elements. For the three dimensional cases we extend the mesh in the $x_3$ direction by 0.00144 m, maintaining an $x_3$-directional resolution of $2d$, and $a$-$d$ of the two dimensional plane doubled in size for less computation cost.

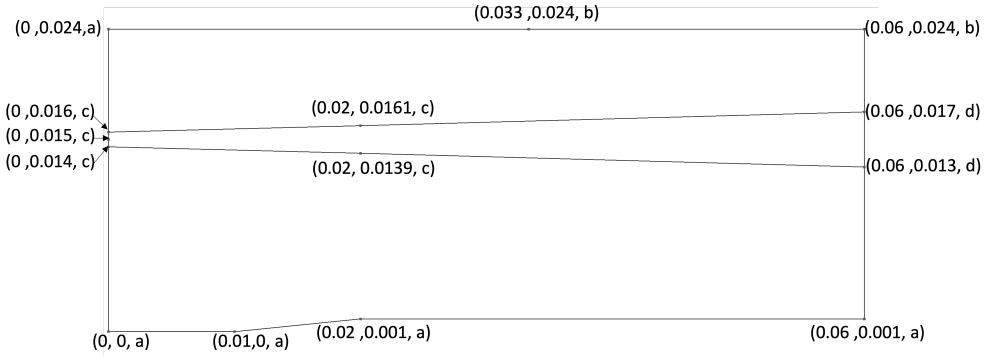


Fig. 2: Diagram of geometry with point locations for mesh construction in gmsh [16]. The third listed parameters, a through d, are the target mesh size at that location.

## 4. RESULTS

Here we present results in two and three dimensions. For the two dimensional cases we use the mesh described above with DG($p = 2$) triangles and DG($p = 2$) tetrahedral for the three dimensional cases. We present a study of length scales that was used to determine the chosen ambient, $L_s$. We then present results for an unsteady two-dimensional test case using an appropriate $L_s$ combined with the perturbation function as described in Equation 24. Finally we extend the two dimensional result into three dimensions.

### 4.1 Effect of Length Scale

Figures 3a to 4b show the results of the mixing layer at four different characteristics lengths, $L_s = (0.005, 0.0025, 0.0005, 0.0001)$ m with no time dependent perturbations, $A_i = 0$, $l = 0$ and ambient center $h_s = 0.00864$ m. For all cases an oblique shock forms on the bottom wall that intersects with the mixing layer. This shock causes a shift in the mixing layer which is shifted again at the downstream reflected shock. As the mixing layer is sharpened by decreasing the length scale an unsteadiness occurs prior to the oblique shock, Figure 4b. The steady solutions are important, especially if one desires to use a steady solver or implicit time marching scheme to produce a steady state solution.

An oblique shock exists at the inflow due to using the hyperbolic tangent function to connect the two conservative states for the fuel and air streams. After these simulations we changed to the hyperbolic tangent function that links the primitive states of mass fraction, temperature, and velocity while preserving pressure equilibrium to avoid the inflow oblique shock. For these test cases the oblique shock also reflects in the domain and interacts slightly with the mixing layer.

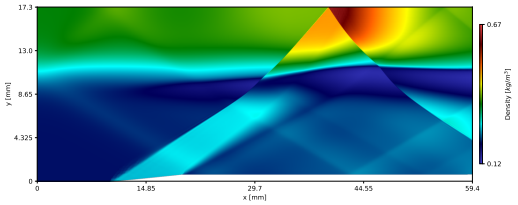

(a) Density of length scale $L_s = 0.005$ m the thickest length scale tested.

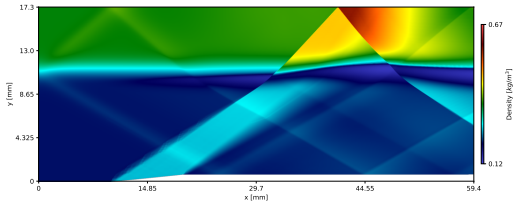

(b) Density of length scale $L_s = 0.001$ m the thickest length scale tested.

Fig. 3— Density of length scale $L_s = 0.005$ and $0.001$ m, the thickest length scales tested. The solutions for these length scales are steady.

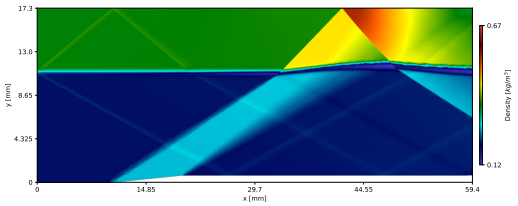

(a) Density of length scale $L_s = 0.0005$ m the thickest length scale tested.

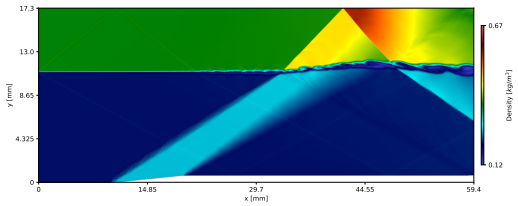

(b) Density of length scale $L_s = 0.0001$ m the thickest length scale tested.

Fig. 4— Density of length scale $L_s = 0.0005$ and $0.0001$ m, the thinnest length scales tested. The solutions for these length scales exhibit unsteady features.

### 4.2 Unsteady Two-Dimensional Results

For the unsteady two-dimensional case, we modified the smallest length scale, $L_s = 0.0001$ m, to include time variation in the inflow boundary conditions with the parameters for $n_t = 4$. We specify wave numbers

$(n_1, n_2, n_3, n_4) = (1, 3, 11, 13)$ and amplitudes $(A_1, A_2, A_3, A_4) = (1 \times 10^{-5}, 5 \times 10^{-5}, 5 \times 10^{-6}, 2.5 \times 10^{-5})$ for a residence time of $t_r = 1.142 \times 10^{-7}$ s. This super imposes several sinusoidal variations in the hyperbolic tangent length scale, stretching the imposed mixing layer thickness. The chosen length scale was already found to have some unsteadiness. DG($p = 2$) triangles were used with the same mesh as used to generate results in Section 4.1.

Figures 5a to 6b show an instantaneous result of a fully developed solution after three residence times. In all four images, unsteady two dimensional features develop at about 7 mm and propagate into the first oblique shock. The shear layer bends upwards after intersecting the first oblique shock and then deflects downwards after intersecting the reflected shock, which is consistent with all results demonstrated previously, Section 4.1. Figure 6a shows intermediate species, $Y_{OH}$. As the reacting shear layer continues downstream more roll-up of the shear layer sheet develops as well as reactivity continues. Figures 5a, 5b,and 6b represent compressible features in the flow. After the oblique, small two-dimensional compression waves propagate off of the shear layers creating unique structure most visible in the numerical Schlieren results, Figure 6b. This case demonstrates our capability to produce solutions with chemically reacting flows, shocks, in high order. The solution is stable maintainable; we stopped running this case in particular at $20t_r$.

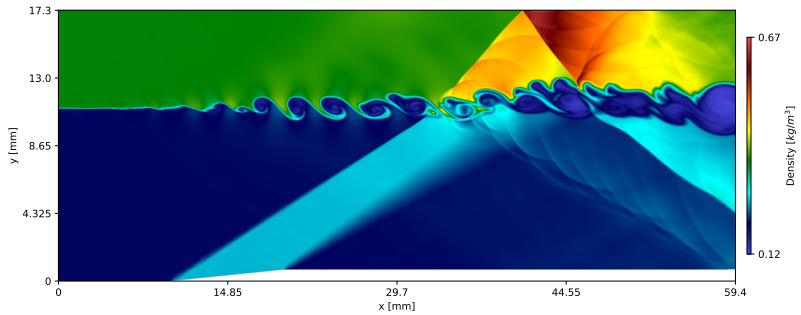


(a) DG($p = 2$) density results for unsteady inflow specification, $(n_1, n_2, n_3, n_4) = (1, 3, 11, 13)$ and $(A_1, A_2, A_3, A_4) = (1 \times 10^{-5}, 5 \times 10^{-5}, 5 \times 10^{-6}, 2.5 \times 10^{-5})$ with $n_t = 4$ and $t_r = 1.142 \times 10^{-7}$ s.

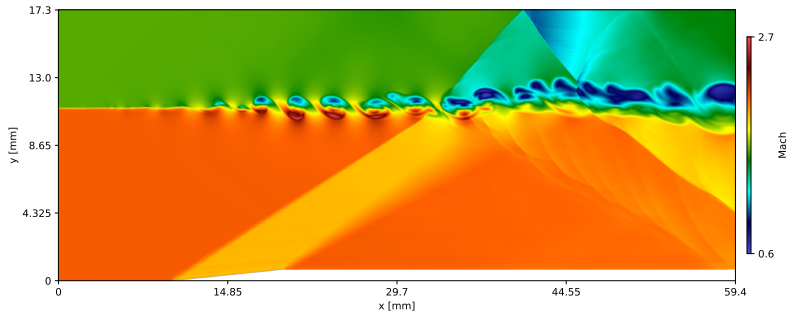


(b) DG($p = 2$) Mach number for unsteady inflow specification, $(n_1, n_2, n_3, n_4) = (1, 3, 11, 13)$ and $(A_1, A_2, A_3, A_4) = (1 \times 10^{-5}, 5 \times 10^{-5}, 5 \times 10^{-6}, 2.5 \times 10^{-5})$ with $n_t = 4$ and $t_r = 1.142 \times 10^{-7}$ s.

Fig. 5— Density and Mach number results for the unsteady chemically reacting hydrogen-air shear layer solution for the unsteady inflow specification, $(n_1, n_2, n_3, n_4) = (1, 3, 11, 13)$ and $(A_1, A_2, A_3, A_4) = (1{\times}10^{-5}, 5{\times}10^{-5}, 5{\times}10^{-6}, 2.5{\times}10^{-5})$ with $n_t = 4$ and $t_r = 1.142{\times}10^{-7}$ s. Unsteady features are increased by the unsteady inflow.

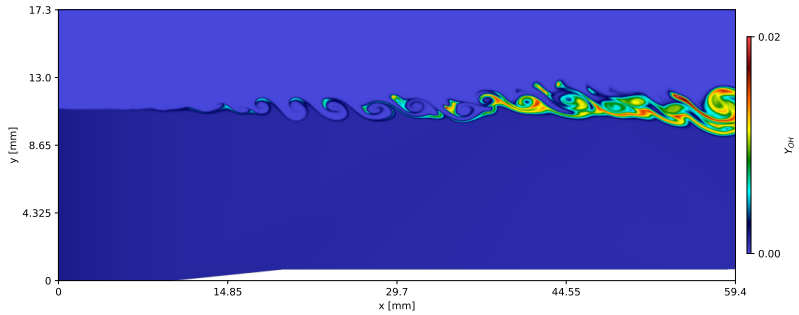


(a) DG($p = 2$) $Y_{OH}$ for unsteady inflow specification, $(n_1, n_2, n_3, n_4) = (1, 3, 11, 13)$ and $(A_1, A_2, A_3, A_4) = (1{\times}10^{-5}, 5{\times}10^{-5}, 5{\times}10^{-6}, 2.5{\times}10^{-5})$ with $n_t = 4$ and $t_r = 1.142{\times}10^{-7}$ s.

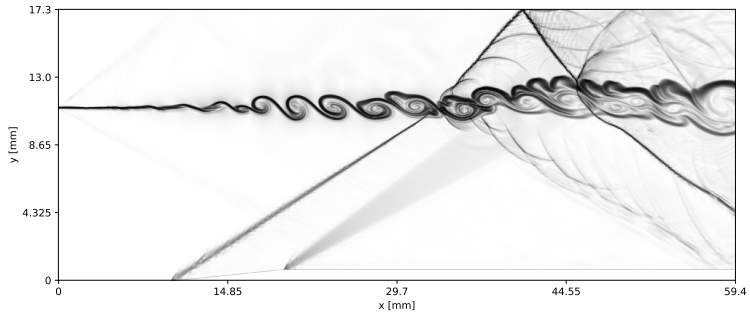


(b) DG($p = 2$) Numerical Schlieren for for unsteady inflow specification, $(n_1, n_2, n_3, n_4) = (1, 3, 11, 13)$ and $(A_1, A_2, A_3, A_4) = (1 \times 10^{-5}, 5 \times 10^{-5}, 5 \times 10^{-6}, 2.5 \times 10^{-5})$ with $n_t = 4$ and $t_r = 1.142 \times 10^{-7}$ s.

Fig. 6— $Y_{OH}$ and numerical Schlieren results for the unsteady chemically reacting hydrogen-air shear layer solution for the unsteady inflow specification, $(n_1, n_2, n_3, n_4) = (1, 3, 11, 13)$ and $(A_1, A_2, A_3, A_4) = (1 \times 10^{-5}, 5 \times 10^{-5}, 5 \times 10^{-6}, 2.5 \times 10^{-5})$ with $n_t = 4$ and $t_r = 1.142 \times 10^{-7}$ s. Unsteady features are increased by the unsteady inflow.

### 4.3 Unsteady Three-Dimensional Results

The two dimensional unsteady case was extended into three dimensions by extruding the planar mesh by 0.00144 m in the $x_3$-direction. The resulting tetrahedrals had a target spacing of 240$\mu$m for the $x_3$-direction edges but matched the meshing specifications as shown in Figure 2. The resulting $x_1$-$x_2$ plane at $x_3 = 0.00144$ m was generated to be periodic with the $x_1$-$x_2$ plane at $x_3 = 0$. Additional $x_3$ perturbations were included via Eq. 25. Figure 7 shows the developed three dimensional result after two residence times, $t_r$. The figure displays an isosurface for $Y_{OH} = 0.017$ and a numerical Schlieren result sampled on an $x_1$-$x_2$ plane at $x_3 = 0.00072$ m along with bounding domain walls. The $Y_{OH}$ isosurface is colored by density to highlight the abrupt compressibility experienced through the oblique shock. A red dashed box is used to highlight a zoomed in area displayed in the lower portion of the figure to further highlight the three dimensional flow features. Compression waves are noticeable in off the oblique and reflecting shocks, however, there may need to be more resolution to fully capture the smaller compression waves. Future work will refine *a-d* for the three dimensional mesh generation and comment on grid resolution. Regardless, these results demonstrate the expected physics and that our method is stable in three dimensions.

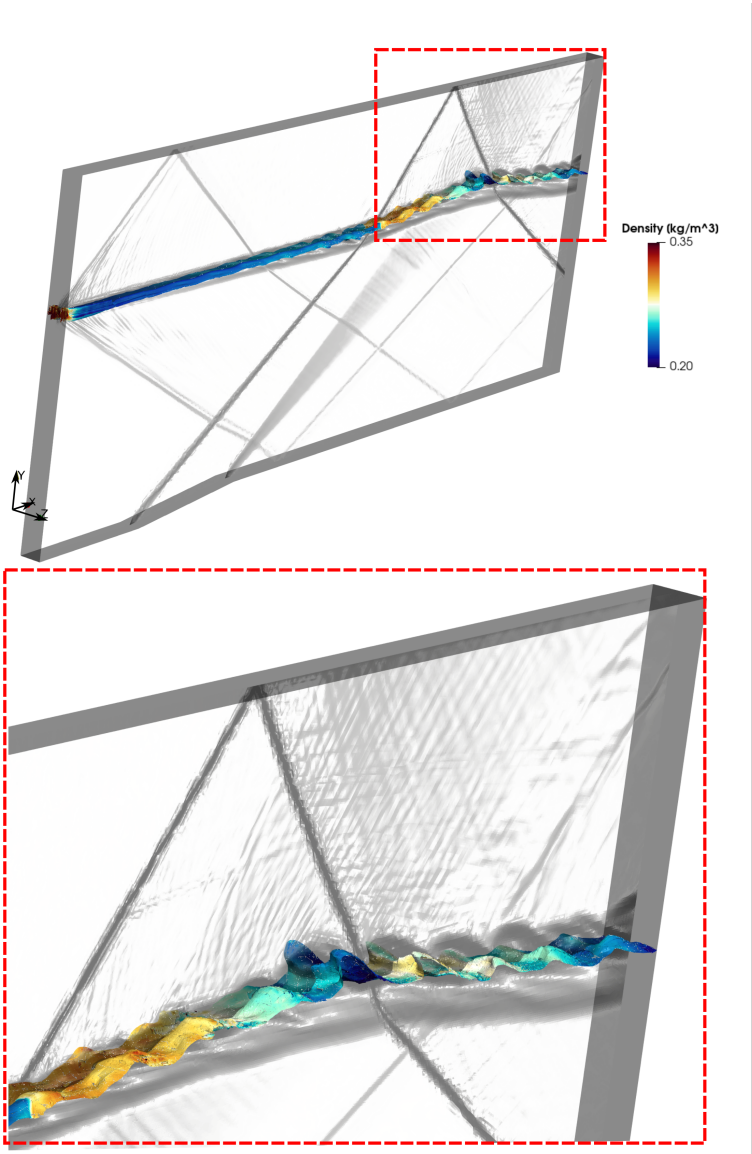


Fig. 7—Three dimensional results showing $Y_{OH}$ isosurface colored by density to demsontrate compression after oblique shock. A numerical Schlieren result at $x$ = 0.00072 m is also displayed showing the oblique shock locations and small compression waves. The zoomed-in red box shows the three dimensionality of the shear layer surface.

### 4.4 Conclusion

We presented the development of a verification test case for the chemically reacting, multi-component Navier-Stokes equations. We determined a configuration that contains the physics of interest to simulating high-speed propulsion devices, namely an oblique shock interacting with a chemically reacting shear layer. We presented the mesh, boundary conditions, and final, reproducible result for both two-dimensional and three-dimensional configurations. For the two-dimensional configuration, we pursued different length scales to determine the effect on specified inflow shear layer thickness. We then presented unsteady two and three dimensional results based on the chosen length scale.

The goal of this presented test case is to help the combustion community in supplying a configuration that any multicomponent chemically reacting compressible Navier Stokes solver should be able to reproduce. Additionally, the accurate simulation and demonstration of these physics with a reproducible test case is important for future work in the field of high speed-propulsion. Simulations were performed using the JENRE® Multiphysics Framework with extensions for numerical stability still currently in development at the Naval Research Laboratory.

## REFERENCES

1. G. Billet and J. Ryan, "A Runge–Kutta discontinuous Galerkin approach to solve reactive flows: The hyperbolic operator," *Journal of Computational Physics* **230**(4), 1064 – 1083 (2011), ISSN 0021-9991, doi:https://doi.org/10.1016/j.jcp.2010.10.025.

2. Y. Lv and M. Ihme, "Discontinuous Galerkin method for multicomponent chemically reacting flows and combustion," *Journal of Computational Physics* **270**, 105 – 137 (2014), ISSN 0021-9991, doi:https://doi.org/10.1016/j.jcp.2014.03.029.

3. R. F. Johnson and A. D. Kercher, "A Conservative Discontinuous Galerkin Discretization for the Chemically Reacting Navier-Stokes Equations," 2020.

4. E. Ching, Y. Lv, P. Gnoffo, M. Barnhardt, and M. Ihme, "Shock capturing for discontinuous Galerkin methods with application to predicting heat transfer in hypersonic flows," *Journal of Computational Physics* **376**, 54–75 (2019).

5. R. Houim and K. Kuo, "A low-dissipation and time-accurate method for compressible multi-component flow with variable specific heat ratios," *Journal of Computational Physics* **230**(23), 8527 – 8553 (2011), ISSN 0021-9991, doi:https://doi.org/10.1016/j.jcp.2011.07.031.

6. P. J. M. Ferrer, R. Buttay, G. Lehnasch, and A. Mura, "A detailed verification procedure for compressible reactive multicomponent Navier–Stokes solvers," *Computers & Fluids* **89**, 88–110 (2014), ISSN 0045-7930, doi:https://doi.org/10.1016/j.compfluid.2013.10.014.

7. R. Hartmann and T. Leicht, "Higher order and adaptive DG methods for compressible flows," in H. Deconinck, ed., *VKI LS 2014-03: 37$^{th}$ Advanced VKI CFD Lecture Series: Recent developments in higher order methods and industrial application in aeronautics, Dec. 9-12, 2013* (Von Karman Institute for Fluid Dynamics, Rhode Saint Genèse, Belgium, 2014).

8. B. J. McBride, M. J. Zehe, and S. Gordon, "NASA Glenn coefficients for calculating thermodynamic properties of individual species (2002).

9. T. Coffee and J. Heimerl, "Transport algorithms for premixed, laminar steady-state flames," *Combustion and Flame* **43**, 273 – 289 (1981), ISSN 0010-2180, doi:https://doi.org/10.1016/0010-2180(81)90027-4.

10. R. J. Kee, J. A. Miller, G. H. Evans, and G. Dixon-Lewis, "A computational model of the structure and extinction of strained, opposed flow, premixed methane-air flames," *Symposium (International) on Combustion* **22**(1), 1479 – 1494 (1989), ISSN 0082-0784, doi:https://doi.org/10.1016/S0082-0784(89)80158-4.

11. C. R. Wilke, "A Viscosity Equation for Gas Mixtures," *J. Chem. Phys* **18**, 517–519 (04 1950), doi:10.1063/1.1747673.

12. S. Mathur, P. K. Tondon, and S. C. Saxena, "Thermal conductivity of binary, ternary and quaternary mixtures of rare gases," *Molecular Physics* **12**, 569–579 (1967), doi:10.1080/00268976700100731.

13. R. Kee, F. Rupley, and J. Miller, "Chemkin-II: A Fortran chemical kinetics package for the analysis of gas-phase chemical kinetics (9 1989).

14. C. K. Westbrook, "Chemical kinetics of hydrocarbon oxidation in gaseous detonations," *Combustion and Flame* **46**, 191 – 210 (1982), ISSN 0010-2180, doi:https://doi.org/10.1016/0010-2180(82)90015-3.

15. N. M. Marinov, C. K. Westbrook, and W. J. Pitz, "Detailed and global chemical kinetics model for hydrogen," *Lawrence Livermore National Lab. (LLNL), Livermore, CA (United States)* (3 1995). URL `https://www.osti.gov/biblio/90098`.

16. C. Geuzaine and J. F. Remacle, "Gmsh: a three-dimensional finite element mesh generator with built-in pre- and post-processing facilities," *International Journal for Numerical Methods in Engineering* (79(11)), 1310–1331 (2009).